Variable-Conductance Behavior in Two-Phase Binary Thermosyphons

P. F. Peterson* and K. Hijikata†
Tokyo Institute of Technology, Tokyo, 152 Japan
and
C. L. Tien‡
University of California, Irvine, California 92717

Two-phase closed thermosyphons using binary mixtures of working fluids can provide equal or superior variable-conductance performance compared to gas-loaded heat pipes. This analysis of binary reflux thermosyphons examines both ideal devices, where no mixing or diffusion occurs in the liquid film and the vapor flow is laminar, and real devices, where some mixing occurs. The total pressure and evaporator temperature change only slightly over wide ranges of power input, reaching equilibrium at values that just allow complete condensation. By introducing two empirical mixing parameters, mixing in the vapor and film can be accounted for, providing good agreement with experimental measurements.

Nomenclature

A = constant, Eq. (9), J/mol
c_p = specific heat, J/kg
C_n = constant, Eq. (11)
D = mass diffusivity, m^2/s
E = diffusion parameter, $\rho_v D h_{lv}/k_l(T_e - T_w)$
f = fugacity, Pa
F = film parameter, $2\rho_l g r_w^3/3\mu_l D$
g = gravitational acceleration, m/s^2
h_{lv} = latent heat, J/kg
k = thermal conductivity, W/mK
Le = Lewis number, $k_v/\rho_v D c_p$
m = film mixing parameter, Eq. (4)
P = absolute pressure, Pa
q = power input, W
r = radial coordinate, m
R = gas constant, J/mol K
Re = Reynolds number, Eq. (18)
Sc_v = Schmidt number, $\mu_v/\rho_v D$
T = absolute temperature, K
u = axial velocity, m/s
v = radial velocity, m/s
x = liquid mole fraction
y = vapor mole fraction
z = axial coordinate, m
δ = film thickness, m
η = vapor mixing parameter
γ = activity coefficient
μ = dynamic viscosity, kg/ms
ν = vapor
ω = mass fraction of more volatile component (R11)
ρ = density, kg/m^3
θ = nondimensional temperature $(T - T_w)/(T_e - T_w)$

Subscripts and Superscripts

a = average
c = condenser
e = evaporator
ex = experimental
i = interface
l = liquid
o = value from previous iteration
n = component
r = reference/residual value
s = saturation value
t = total
w = wall
wm = well-mixed film
um = unmixed film
∞ = centerline
$*$ = nondimensional quantity

Introduction

KATZOFF[1] first noted that small amounts of noncondensable gas can provide simple thermostatic control for heat pipes. Since then, extensive efforts have improved the understanding and prediction of the mechanisms controlling gas-loaded device performance and creating their useful constant-temperature behavior.[2-5] With gas loading, increasing the power input raises the system pressure, which compresses the noncondensable gas accumulated at the need of the condenser, exposing more condenser surface area and controlling the evaporator temperature increase. Recently Hijikata et al.[6] found that similar variable-conductance behavior can occur in reflux thermosyphons, even without noncondensable gases, when the thermosyphon evaporator is charged with a liquid pool of R113 and R11. With this binary mixture, a shut-off zone was observed at the end of the condenser, as illustrated schematically by Fig. 1. As the power input was changed, the length of the shut-off zone also changed, such that the system pressure and evaporator temperature remained virtually constant. This constant-temperature behavior occurred even though no gas reservoir or active control was provided as is commonly required in gas-loaded devices.

Binary film condensation on flat plates has received considerable attention,[7-9] and convective filmwise binary condensation has also been investigated.[10] In one of the earliest studies of binary heat pipes, Tien and Rohani[11] provided analysis and experimental results for a wicked heat pipe using a water/

Presented as Paper 89-1746 of the 24th AIAA Thermophysics Conference, Buffalo, NY, June 12-14, 1989; received March 20, 1989; revision received Aug. 22, 1989.

*JSPS Fellow, Department of Mechanical Engineering Science. Member AIAA.
†Professor, Department of Mechanical Engineering Science; currently at University of California, Berkeley, Department of Nuclear Engineering. Member AIAA.
†Distinguished Professor, Department of Mechanical Engineering. Fellow AIAA.

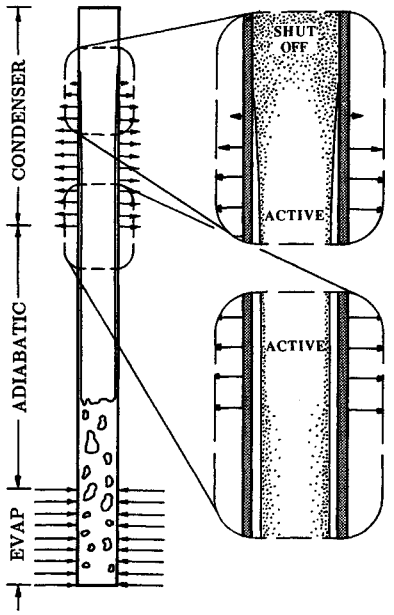

Fig. 1 Schematic of binary thermosyphon.

ethanol mixture. They did not observe constant pressure behavior, due to the evaporator geometry and nonideal fluid combination, and thus their model did not account for the potential shut off of the condenser. With a wicked evaporator, the vapor concentration exiting the evaporator is a function of the geometry and power level, whereas, for pool boiling in a thermosyphon, the vapor concentration remains relatively constant. Hijikata et al.[6] used an integral technique to analyze the binary thermospyhon. For binary condensation, the concentration boundary-layer thickness varies strongly with the condensation rate, so their assumption of a parabolic concentration required the introduction of an empirical correction factor to match the experimental data.

This work solves directly the parabolic forms of the species and energy equations for the concentration and temperature boundary layers. This permits exact satisfaction of the complex boundary conditions and inclusion of empirical corrections for mixing in the liquid film and the vapor. These solutions identify the primary control mechanism in binary devices. Suction from condensation thins the concentration boundary layer and decreases the mass transfer resistance, giving a nonlinear response to changes in total pressure. Only one pressure permits complete condensation, with physically unreasonable behavior occurring at other pressures.

This work improves the understanding of binary thermosyphons by introducing an improved phase equilibrium relationship for binary refrigerant mixtures, better models for the liquid film and the vapor, and nondimensionalization and numerical solution of the film and vapor governing equations. The special considerations required for the adiabatic and condensing sections are discussed. From the results of the model, a detailed explanation of the device behavior is provided. The primary assumptions used concern mixing in the film and vapor. Because these assumptions require introduction of empirical film and vapor mixing parameters, further experimental results are required before the model can be applied for binary thermosyphon design.

Liquid Film Modeling

It is difficult to determine the concentration distribution in a binary liquid film, due to the complex mass transfer in the liquid. However, there are two limiting behaviors that can be expected in falling films of binary liquid mixtures, which provide boundary conditions for the vapor space conservation equations. In one limit, the film is well mixed by convection and diffusion, and in the other limit, no convective mixing occurs and diffusion is negligible. Both limits are examined here, and the behavior of real devices is shown to lie between the two limiting cases.

Well-Mixed Film

If the falling film is well mixed, then the concentration across the film is uniform. Since, under steady conditions, mass conservation at any point requires that the flow rate of each species in the liquid film must equal that in the vapor, the concentration in the film is equal to the average concentration in the adjoining vapor

$$\omega_{v,a} = \omega_{l,a} = \omega_{li} = \int_0^{r_w} \omega_v u r \, dr \Big/ \int_0^{r_w} u r \, dr \tag{1}$$

where $\omega_{v,a}$ and $\omega_{l,a}$ are the average vapor and liquid mass concentrations of the more volatile component (R11), u is the axial velocity, r the radial coordinate, and z the axial coordinate. Axial diffusion is neglected, and the liquid film is assumed sufficiently thin, so that the liquid interface radius r_i approximately equals the inner wall radius r_w. This liquid interface concentration ω_{li}, combined with a phase equilibrium relationship and energy conservation, defines the gas mass concentration at the liquid/vapor interface, and thus provides the necessary boundary condition for the species equation.

Unmixed Film

When no convective mixing or diffusion occurs in the liquid film, or when a capillary wicking structure is provided and liquid diffusion is small, the liquid interface concentration is independent of the concentration distribution inside the film. Then, species conservation at the interface requires that

$$\omega_l \rho_l v_{li} = \omega_v \rho_v v_{vi} - \rho_v D[\partial \omega_v / \partial r]_i \tag{2}$$

where diffusion in the liquid film is neglected. Noting that total mass conservation at the interface requires that $\rho_l v_{li} = \rho_v v_{vi}$, a simpler form emerges

$$D[\partial \omega_v / \partial r]_i = v_{vi}(\omega_v - \omega_l) \tag{3}$$

Adiabatic Section

Since in the adiabatic section, no heat transfer occurs across the film, the wall temperature T_w is virtually equal to the vapor/liquid interface temperature T_i. Because no condensation or evaporation occurs at the interface, convection is negligible ($v_{vi} = 0$) and any effects of diffusion and mixing in the film are magnified. When the unmixed model is applied, then Eq. (3) gives $[\partial \omega_v / \partial r]_i = 0$. Thus, for the unmixed case, no mass transfer occurs and the interface concentration must remain equal to the concentration leaving the evaporator, so the interface temperature T_i must equal the evaporator temperature. Experiments[6] show that the interface temperature actually drops through the adiabatic section, demonstrating that some mixing and diffusion does occur in the liquid film. However, the well-mixed model greatly overpredicts the mixing effects.

For the adiabatic section, a simple combined film-mixing model can be developed. Mass conservation requires that the average liquid concentration equal the average vapor concentration any any cross section, as given by Eq. (1). For uniformly well-mixed liquid film, the liquid concentration at the interface equals this average value, $\omega_{li} = \omega_{va}$, and the vapor interface concentration is the equilibrium value $\omega_{vi} = \omega_{wm} = \omega_v(\omega_{li} = \omega_{va})$. Conversely, for an unmixed film, the slope of the concentration at the interface is zero, and the interface concentration equals the average vapor concentration $\omega_{vi} = \omega_{um} = \omega_{va}$. In the adiabatic section, the actual vapor in-

terface concentration lies somewhere between the well-mixed and unmixed values:

$$\omega_{vi} = m\omega_{wm} + (1 - m)\omega_{um} \tag{4}$$

By iterative selection of the film mixing parameter m, it is possible to match the experimentally observed adiabatic wall temperatures.

Condenser Section

It can be shown that for uniform concentration profiles entering the condenser and for relatively high condensation rates, the unmixed and well-mixed models provide identical results, a conclusion observed and applied in other multicomponent condenser problems.[12] But if the radial concentration profile entering the condenser is nonuniform, as when mass transfer occurs in the adiabatic section, or when the condensation rate is relatively low, then the well-mixed and unmixed film models predict different condensation rates.

No simple combined mixing model is available for the condensing section. This presents no significant difficulty, since the experimental results show that the interfacial mass flux, due to mixing and diffusion in the adiabatic section liquid film, is two orders of magnitude less than the interfacial flux due to condensation in the condenser section. Phase change in the condenser is primarily thermally driven; in the adiabatic section it is concentration induced. With condensation, the interfacial convection in the liquid film dominates diffusion, and the unmixed model can be applied with good accuracy.

Film Energy Balance

The film energy balance provides additional boundary conditions for the vapor space conservation equations. The balance neglects axial conduction in the pipe wall and convection in the liquid film. The contribution of latent heat is assumed to be much greater than convection of sensible heat and conduction in the vapor phase. In addition, the heat of mixing is neglected. Since the vapor conduction, transport of sensible heat, and heat of mixing are also neglected, the assumption of constant latent heat h_{lv} automatically satisfies the overall energy balance. Then the energy balance for the film can be written

$$\frac{(T_i - T_w)k_l}{\delta} = \rho_v v_{vi} h_{lv} \tag{5}$$

where T_i is the vapor/liquid interface temperature, T_w the wall temperature, k_l the liquid thermal conductivity, and h_{lv} the latent heat. When a capillary wicking structure is provided, δ is a constant, and an effective matrix/liquid thermal conductivity must be used. For a falling film, assuming that Nusselt's solution for the film thickness can be applied and $\delta \ll r_w$, neglecting vapor shear, and noting that an overall mass balance at any axial location requires that the vapor flow rate equal the liquid flow rate, the film thickness δ at any point can be related to the vapor flux

$$2\pi\rho_v \int_0^{r_w} ur\, dr = 2\pi\rho_l(\rho_l - \rho_v)g r_w \delta^3/3\mu_l \tag{6}$$

where g is the gravitational constant and μ_l the liquid dynamic viscosity.

Vapor Modeling

The two primary phenomena of interest in the binary condenser are the vapor diffusion and the nonlinear effect of phase equilibrium on the boundary conditions. To simplify the computation while focusing on these most important features, the momentum equations were eliminated by assuming reasonable axial velocity profiles. The requirements of mass conservation were then satisfied by assuming constant mass density and selecting appropriate values for the radial velocity. Both parabolic and uniform axial velocity profiles were investigated, with the type of profile selected having only a small effect on the results.

Though the vapor flows studied here were in the laminar or transition regions, the experimentally measured centerline temperature drops significantly. This drop suggests that unsteady pool boiling causes significant mixing in the vapor, since with purely laminar flow the boundary layers do not reach the centerline and no temperature drop would be expected. To account for this vapor mixing, the species and energy equations were modified so that the effective diffusivities increased linearly from the molecular values at the vapor/liquid interface to maximum values of $(1 + \eta)D$ and $(1 + \eta)k_v/\rho_v c_p$ at the pipe centerline. Here η is an adjustable mixing parameter, determined iteratively and assumed to remain constant throughout the condenser. This rather ad hoc assumption provided good agreement with the experimental data of Hijikata et al.[6]

The parabolic forms of the conservation equations allow use of a marching technique from the evaporator exit. Use of the parabolic forms is justified, except at axial velocities $ur_w/D < 10$, since the ratio of axial diffusion to convection is never more than 0.2%, and commonly much less. Runs where an iterative technique, with the full elliptic equations, was employed in the low-velocity region showed only a small change from the parabolic solution, since condensation in the higher velocity region controls device performance. Thus, the species conservation equation becomes

$$v\frac{\partial \omega_v}{\partial r} + u\frac{\partial \omega_v}{\partial z} = D\frac{1}{r}\frac{\partial}{\partial r}\left\{r[1 + (1 - r/r_w)\eta]\frac{\partial \omega_v}{\partial r}\right\} \tag{7}$$

and the energy conservation equation becomes

$$v\frac{\partial T}{\partial r} + u\frac{\partial T}{\partial z} = \frac{k_v}{\rho_v c_p}\frac{1}{r}\frac{\partial}{\partial r}\left\{r[1 + (1 - r/r_w)\eta]\frac{\partial T}{\partial r}\right\} \tag{8}$$

where k_v is the vapor thermal conductivity.

Phase Equilibrium

Phase equilibrium requirements provide the final boundary condition required for the vapor space conservation equations. In general, calculation of equilibrium liquid and vapor phase concentrations for binary mixtures requires experimental data for the mixture, in addition to pure-component property data. In particular, the liquid fugacities can deviate greatly from those of an ideal liquid. The experimental work used to validate the model developed here also provides information on the mixture behavior. During operation of the experiment, both the total pressure P_{ex} and the evaporator saturation temperature at the top of the liquid pool T_{ex} were measured. Thus, combined with the known molar concentration in the liquid pool, the set y, P, and T are known for a point on the mixture equilibrium curve.

Sophisticated model for refrigerant mixture equilibrium are available.[13] However, since the operating pressures were relatively low here, a simpler equilibrium relationship is used. The equilibrium relationship is designed to provide the best fit over the range of conditions found in the thermosyphon. Thus, the constants in the relationship are chosen, based on tabular data for a reference pressure P_r very near the given operating pressure, and also for the limiting temperatures T^s_{r1} and T^s_{r2}, the pure component saturation temperatures at P_r.

For an equilibrium mixture,[14] the vapor and liquid-phase fugacities for each component n must be equal, $f^v_n = f^l_n$. The liquid phase fugacity can be expressed as $f^l_n = \gamma_n x_n P^s_m$, where γ_n is the activity coefficient. The simplest expression for the activity coefficient, besides setting it equal to unity, is the

two-suffix Margules equation,

$$\ln\gamma_1 = \frac{A}{RT}x_2^2, \qquad \ln\gamma_2 = \frac{A}{RT}x_1^2 \tag{9}$$

where R is the gas constant and T the absolute temperature. The constant A is determined from experimental data for the mixture and is a weak function of temperature. Here A is assumed to remain constant over the range between the two limiting temperatures T_{r1}^s and T_{r2}^s. The assumption of ideal-gas behavior in the vapor phase allows the use of the Clausius-Clapeyron relation for the saturation pressure and temperature of each component. To provide the best fit over the range of temperatures encountered in the thermosyphon, and to avoid the difficulty of selecting an averaged value for the latent heat, the relationship is written so that it can be fit to the exact saturation pressures near the two limiting temperatures. This provides a more realistic approximation for the range of pressure and temperature encountered in the specific device. Hence, it follows

$$P_n^s = P_r \exp[C_n(1 - T_{rn}^s/T)] \tag{10}$$

The constants C_n, instead of being related to an average value of the latent heat, are found more accurately by fitting saturation pressure data

$$C_1 = \frac{\ln(P_1^s/P_r)}{(1 - T_{r1}^s/T_{r2}^s)} \tag{11a}$$

$$C_2 = \frac{\ln(P_2^s/P_r)}{(1 - T_{r2}^s/T_{r1}^s)} \tag{11b}$$

where P_1^s is the saturation pressure of component 1 at temperature T_{r2}^s and P_2^s at T_{r1}^s.

The ideal-gas assumption also allows the use of a simplified relationship for the vapor-phase fugacity, $f_n^v = y_n P_t$, where y_n is the vapor mole fraction and P_t is the total pressure. Then, simple expressions for the liquid- and vapor-phase equilibrium mole concentrations, respectively, result in

$$x_1 = \frac{(P_t/P_r)\exp[-G_2(T)] - 1}{\exp[G_1(T) - G_2(T)] - 1} \tag{12}$$

$$y_1 = \frac{(P_r/P_t)\exp[G_2(T)] - 1}{\exp[G_2(T) - G_1(T)] - 1} \tag{13}$$

where

$$G_1(T) = C_1\left(1 - \frac{T_{r1}}{T}\right) + \frac{Ax_2^2}{RT} \tag{14a}$$

$$G_2(T) = C_2\left(1 - \frac{T_{r2}}{T}\right) + \frac{Ax_1^2}{RT} \tag{14b}$$

The constant A can be set equal to zero or it can be found by fitting a set of experimentally measured P_t, T, and y_1. Neither Eq. (12) nor (13) is explicit in T, but if x_1 or y_1 is specified, a Newton-Raphson iterative scheme converges rapidly to the desired value of T. Furthermore, Eq. (13) can be differentiated in a straightforward manner to obtain an explicit expression for $\partial y_1/\partial T$, which proves to be useful in the numerical analysis. Figure 2 shows the resulting phase diagram for $A = 0$ with $P_t = 107$. Experimental data for several runs with the R11/R113 mixture gave some scatter in the value of A, primarily due to uncertainty in defining the top point of the pool. However, the resulting phase equilibrium diagrams agreed with the ideal solution ($A = 0$) within 1°C, and, thus, the ideal solution used for the thermosyphon analysis.

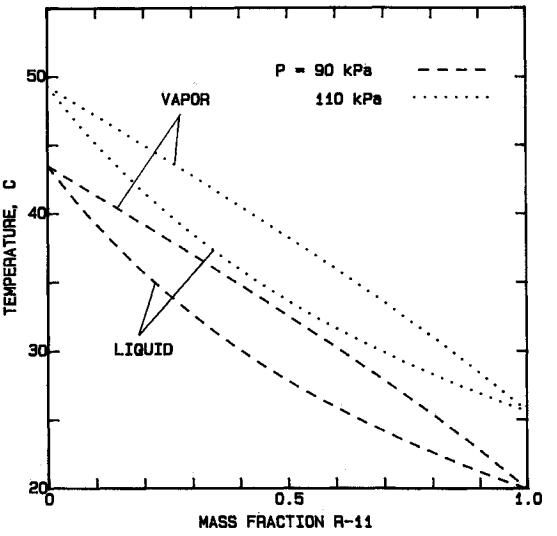

Fig. 2 Binary phase equilibrium for R11/R113.

Nondimensional Equations

To simplify and help generalize the results, the equations are nondimensionalized with the following relationships:

$$\theta = \frac{T - T_w}{T_e - T_w}$$

$$v^* = \frac{vr_w}{D} \quad u^* = \frac{ur_w}{D} \quad r^* = \frac{r}{r_w} \quad z^* = \frac{z}{r_w} \quad \delta^* = \frac{\delta}{r_w} \tag{15}$$

$$E = \frac{\rho_v D h_{lv}}{k_l(T_e - T_w)} \quad F = \frac{2\rho_l g r_w^3}{3\mu_l D} \quad Sc_v = \frac{\mu_v}{\rho_v D} \quad Le = \frac{k v}{\rho_v D c_p}$$

Then the nondimensional form of the energy balance, Eq. (5), becomes

$$\theta = E v_i^* \delta^* \tag{16}$$

The numerical solution is more difficult for the unmixed film model in the condenser. For higher condensation rates, the solution requires a high initial guess for the interface temperature and a sufficiently fine grid near the wall to insure convergence on the correct interface concentration. This initial temperature guess provides initial values of δ_o^i, $\omega_{li,o}$, $\omega_{vi,o}$, and v_i^* for use in Eq. (21). Then the finite difference form of the species equation, subject to this linearized mixed boundary condition, can be solved directly with a tridiagonal-matrix algorithm, and a new value of ω_{vi} obtained. From the new concentration, ω_{vi} phase equilibrium gives a new interface temperature θ_o and the other variables follow. The procedure can be repeated until the values of the nondimensional temperature obtained from phase equilibrium agree with those from the film energy balance within 10^{-4}. Normally, about seven iterations are required. For the calculations presented here, the adiabatic section was subdivided axially into 30 segments, and the condenser into 100. Doubling the number of segments changed the calculated nondimensional interface and centerline temperature by under 0.5%. For all calculations, property values for pure R113 were used, evaluated at the average of the R113 and R11 saturation temperatures.

Results

Figure 3 shows centerline and interface temperature profiles for various total pressures for an ideal binary thermosyphon, with no mixing or diffusion in the liquid film and laminar flow

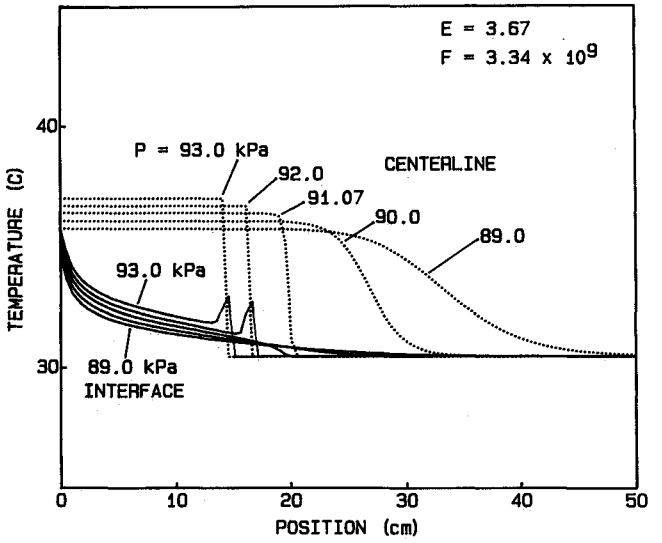

Fig. 3 Axial temperature profiles at different total pressures for an ideal thermosyphon.

in the vapor ($m = \eta = 0$). The parameter values used are the same as those investigated experimentally by Hijikata et al.[6] The power input is 50 W, and a linear velocity profile is assumed. An ideal device will equilibrate to $P_t = 91.07$. The condensation rate reacts very strongly to increasing system pressure. Suction from this condensation thins the diffusion boundary layer, decreasing the diffusion resistance and magnifying the effect on the condensation rate. At sufficiently high condensation rates, the diffusional resistance vanishes, and the mixture behaves like a pure vapor. Here in the small pressure range from $P = 89$ to 93 kPa, corresponding to an evaporator temperature increase of less than 1.5°C, the active condenser area is more than halved.

Figure 4 shows the mechanism directing the ideal device operating pressure to $P_t = 91.07$. At lower pressures, the axial mass flow rate is not zero at the end of the condenser; rather, it reaches an asymptotic limit as $z \to \infty$. At these lower pressures, the interface temperature drops to the cooling medium value before complete condensation can occur, giving the physically unreasonable result that mass flow exists at infinity. The dotted line in Fig. 4 shows the relationship between this asymptotic mass flow rate, denoted by the residual velocity u_r^*, and the guessed pressure, at a power input of 50 W. The

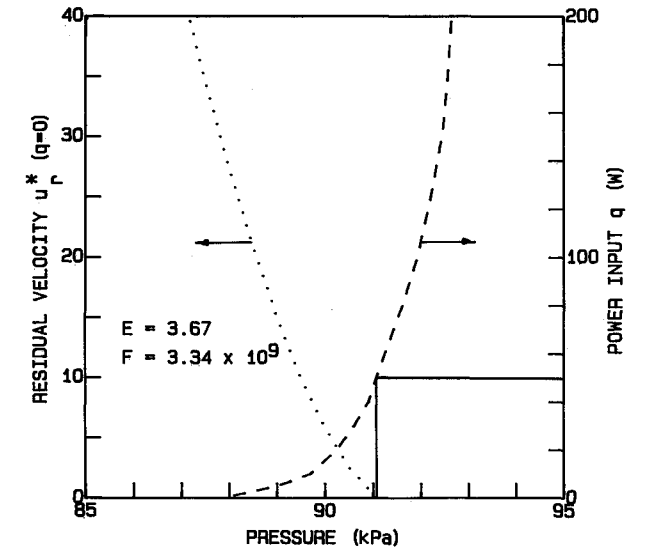

Fig. 4 Residual velocity vs pressure for $q = 50$ W (dotted line) and power level vs pressure (dashed line).

physically realistic situation occurs at the point where $u_r^* = 0$, at a pressure of 91.07 kPa. This is the pressure an ideal thermosyphon would naturally seek at a power level of 50 W, when the condenser is sufficiently long. The residual velocity also helps explain the abrupt drop in the centerline temperature that occurs at higher pressures. These high-pressure solutions are appropriate for shorter condensers. For instance, a 14 cm long ideal condenser would operate at a pressure of 93 kPa. Computations with a parabolic rather than linear velocity profile caused the calculated equilibrium pressure to decrease by 0.9 kPa, a relatively small change, showing the insensitivity of the model to the assumed velocity profile.

The film thickness, Eq. (6), is

$$F\delta^{*3} = 2\int_0^1 u^* r \, \mathrm{d}r^* = u_a^* \tag{17}$$

where u_a^* is the average vapor velocity. The vapor and liquid Reynolds numbers are related to this quantity in a simple manner:

$$Re_v = 2u_a^*/Sc_v \qquad Re_l = Re_v\mu_v/\mu_l \tag{18}$$

For the well-mixed film model, the boundary condition for the species equation, Eq. (1), becomes

$$\omega_{v,a} = \omega_{l,a} = \omega_{l,i} = 2\int_0^1 \omega_v u^* r^* \mathrm{d}r^*/u_a^* \tag{19}$$

Likewise, for the unmixed model, Eq. (3) becomes

$$[\partial\omega_v/\partial r^*]_i = v_i^*(\omega_v - \omega_l) = \frac{\theta}{E\delta^*}(\omega_v - \omega_l) \tag{20}$$

In the adiabatic region, this reduces to $[\partial\omega_v/\partial_r^*]_i = 0$.

When the governing equations are solved numerically, Eq. (20) can be linearized via a Taylor series expansion and solved iteratively:

$$\frac{E\delta_o^*}{(\omega_{vi} + \omega_l)_o}\left[\frac{\partial\omega_v}{\partial_r^*}\right]_i = \theta_o + (\omega_{vi} - \omega_{vi,o})\left[\frac{\partial\theta}{\partial\omega_v}\right]_o \tag{21}$$

where the subscript o indicates the value calculated from equilibrium considerations using ω_{vi} from the previous iteration. The derivative $(\partial\theta/\partial\omega_v)_o$ comes from Eq. (13).

The nondimensional forms of the species and energy equations are

$$v^*\frac{\partial\omega_v}{\partial r^*} + u^*\frac{\partial\omega_v}{\partial z^*} = \frac{1}{r^*}\frac{\partial}{\partial r^*}\left\{r^*[1 + (1 - r^*)\eta]\frac{\partial\omega_v}{\partial r^*}\right\} \tag{22}$$

and

$$v^*\frac{\partial\theta}{\partial r^*} + u^*\frac{\partial\theta}{\partial z^*} = Le\frac{1}{r^*}\frac{\partial}{\partial r^*}\left\{r^*[1 + (1 - r^*)\eta]\frac{\partial\theta}{\partial r^*}\right\} \tag{23}$$

Numerical Procedure

The species and energy equations were converted to finite-difference equations, using the control volume approach.[15] Because the diffusion boundary layer can be extremely thin in the active region, a highly nonuniform grid was used, with half the nodes located very close to the liquid/vapor interface and spaced in a nonuniform exponentially increasing pattern away from the wall, while the other half of the nodes were spaced uniformly in the center. The parabolic form of the governing equations allowed an axial marching procedure, starting from the top of the liquid pool.

The numerical solution is relatively easy in the adiabatic section for all of the film models, since the slope or absolute value of the concentration at the vapor/liquid interface is

given directly. Only about four iterations with a tridiagonal-matrix algorithm[15] are required at each axial location to correct the film thickness δ and suction velocity v_i^*, so that the calculated nondimensional interface temperature changes by less than 10^{-6}.

At different power levels, the system seeks different equilibrium pressures, as given by the dashed curve in Fig. 4. The results are valid for power levels greater than 5 W, since, for $u^* > 10$, the ratio of axial diffusion to convection is less than 0.01, justifying the assumed parabolic forms of the conservation equations. For the higher power levels, the low velocity region where axial diffusion is important is short and does not significantly affect the predicted operating pressure. Though the dashed line shows that the total pressure does increase with increasing power input, the corresponding change in evaporator temperature from 5 to 200 W is less than 1.1°C. This can be considered excellent passive variable-conductance performance.

The total pressures measured by Hijikata et al.,[6] though still virtually constant with changes in power, are about 7% higher than those predicted for an ideal binary thermosyphon. This increased pressure can be attributed primarily to significant mass transfer in the relatively long adiabatic section. However, when the ideal model is modified to account for mixing and diffusion in the adiabatic-section liquid film and for mixing in the vapor, good agreement between the model and experiments can be obtained. To do this, the measured liquid concentration and centerline temperature at the top of the liquid pool ($x_{R11} = 0.24, z = 0.45\ m$) were used as inlet conditions for the model. For a guessed value of the vapor mixing parameter η, the film mixing parameter m was then adjusted until the residual velocity u_f^* equaled zero. Repeating this procedure gave a set of equilibrium values for η and m. Because of the vapor mixing and the suction in the condenser, a linear velocity profile was used.

Figure 5 compares analytic centerline and interface temperatures for two equilibrium sets of η and m with measured centerline and wall temperatures from Hijikata et al.,[6] for a power level of 70.7 W. These experiments used a 162-cm-long, 2.6-cm-i.d. vertical thermosyphon, filled with a liquid pool of 24 mole percent R11 and 76 mole percent R113. The theory predicts the centerline and adiabatic section interface temperatures well. The film is closer to being nonmixed, as shown by the relatively small value of the film mixing parameter m. However, the integrated effect of this mixing over the length of the adiabatic section is rather large, since, with $m = 0$, the centerline and interface temperatures would remain constant in the adiabatic section.

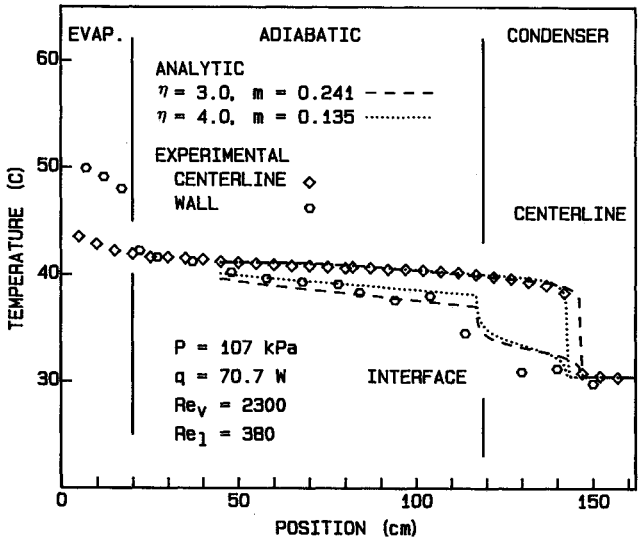

Fig. 5 Experimental[6] and analytic temperature profiles for binary thermosyphon.

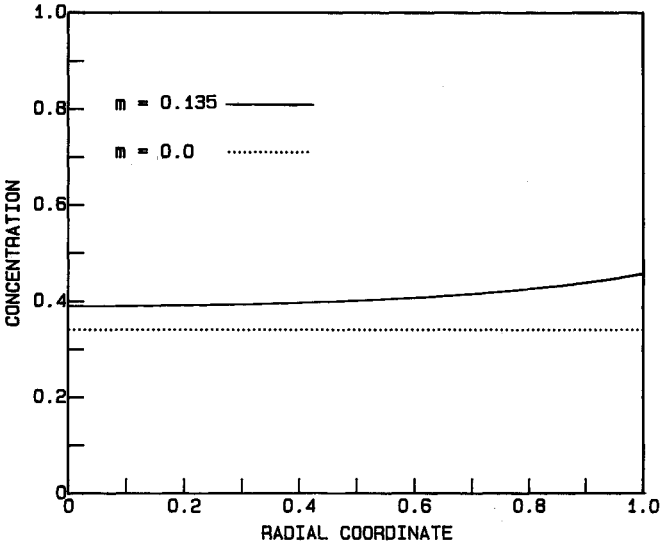

Fig. 6 Mass concentration profiles entering condenser section for no mixing and partial mixing in liquid film in adiabatic section.

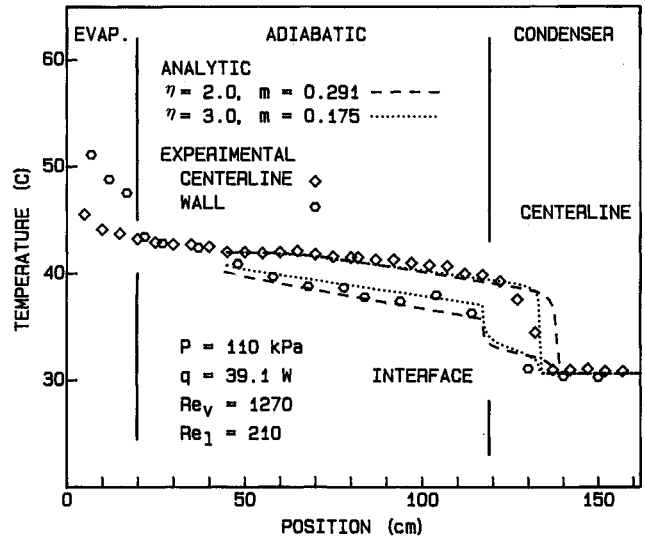

Fig. 7 Experimental[6] and analytic temperature profiles for binary thermosyphon.

Figure 6 explains the large effect of the adiabatic section observed in the previous figure, by comparing the concentration profiles at the exit of the condenser for the case with film mixing ($m = 0.09$) and no mixing ($m = 0$). Mass transfer in the adiabatic section significantly raises the concentration of the more volatile component. When condensation occurs with this higher concentration, the interface temperature must be lower, and, thus, more condenser surface area is required to condense the vapor.

Figure 7 provides a comparison of experimental and analytic predictions at a significantly lower power input. Good agreement for the adiabatic interface temperature is again obtained. The centerline temperature deviates more. Here, the vapor Reynolds number is well within the laminar region, so the mixing due to the unsteady pool boiling can decrease axially and the assumption that the vapor mixing parameter is constant along the length of the adiabatic section may not be valid. For these experiments,[6] the pressure was observed to decrease slightly as power was increased, contrary to the behavior of an ideal device, as illustrated in Fig. 4. This suggests that, with a carefully selected adiabatic length, the change of pressure with power input can be virtually canceled.

Conclusions

Using the parabolic forms of the species and energy equations subject to appropriate boundary conditions and film models, solutions for the performance of binary thermosyphons can be obtained. For an ideal boundary thermosyphon, where no mixing or diffusion occurs in the liquid film and the vapor flow is laminar, the equilibrium evaporator temperature and total pressure can be determined directly. When mixing occurs in the liquid film or the vapor, then two empirical mixing parameters, m and η, must be introduced. By adjusting these parameters, it is possible to match closely experimentally measured centerline and wall temperature profiles.

The phase equilibrium relationships, film models, and vapor governing equations presented here provide a basis for understanding binary device behavior and the mechanisms responsible for binary variable-conductance behavior. In real devices, film mixing and diffusion in the adiabatic section and mixing in the vapor alter device behavior, as accounted for by mixing parameters. Additional experimental data are needed to provide a basis for determining the value of these mixing parameters before the model can be applied to design of binary variable-conductance devices. Pool boiling of binary mixtures in a thermosphyon evaporator can be easily modeled, but evaporation in a wicked evaporator is considerably more complicated and will require further attention. Wicking of the condenser section could potentially suppress film mixing and insure ideal behavior even a high power levels.

Acknowledgments

Support from the Tokyo Institute of Technology Centennial Memorial Fund, the Japan Society for the Promotion of Science Fellowship Programs, and also the National Science Foundation through Grant CBT-8807174 is sincerely appreciated.

References

[1]Katzoff, S., "Heat Pipes and Vapor Chambers for Thermal Control of Spacecraft," *Thermophysics of Spacecraft and Planetary Bodies*, edited by G. B. Heller, Academic, New York, 1967, pp. 225–234.

[2]Edwards, D. K., and Marcus, B. D., "Heat and Mass Transfer in the Vicinity of the Vapor-Gas Front in a Gas-Loaded Heat Pipe," *Journal of Heat Transfer*, Vol. 94, Ser. C, No. 2, 1972, pp. 155–162.

[3]Hijikata, K., Chen, S. J., and Tien, C. L., "Non-Condensible Gas Effect on Condensation in a Two-Phase Closed Thermosyphon," *International Journal of Heat and Mass Transfer*, Vol. 27, No. 8, 1984, pp. 1319–1325.

[4]Bobco, R. P., "Variable Conductance Heat Pipes: a First Order Model," *Journal of Thermophysics and Heat Transfer*, Vol. 1, No. 1, 1987, pp. 35–42.

[5]Peterson, P. F., and Tien, C. L., "Numerical and Analytical Solutions for Two-Dimensional Gas Distribution in Gas-Loaded Heat Pipes," *Journal of Heat Transfer,* Vol. 111, 1989, pp. 598–604.

[6]Hijikata, K., Hasegawa, H., and Nagasaki, T., "A Study on a Variable-Conductance Heat Pipe Using a Binary Mixture," *Proceeding of the XX International Symposium of the International Center for Heat and Mass Transfer*, Hemisphere, New York, 1988.

[7]Sparrow, E. M., and Marschall, E., "Binary, Gravity-Flow Film Condensation," *Journal of Heat Transfer*, Vol. 91, Ser. C, No. 2, 1969, pp. 205–211.

[8]Denny, V. E., and Jusionis, V. J., "Effects of Forced Flow and Variable Properties on Binary Film Condensation," *International Journal of Heat and Mass Transfer*, Vol. 15, 1972, pp. 2143–2153.

[9]Hijikata, K., Mori, Y., Himeno, N., Ingawa, M., and Takahasi, K., "Free Convective Condensation of a Binary Mixture of Vapors," *Proceedings of the 8th International Heat Transfer Conference*, Vol. 4, edited by C. L. Tien et al, Hemisphere, New York, Aug. 1986, pp. 1621–1626.

[10]Mochizuki, S., Yagi, Y., and Yang, Y. J., "Convective Filmwise Condensation of Nonazetropic Binary Mixtures in a Vertical Tube," *Journal of Heat Transfer*, Vol. 106, No. 3, 1984, pp. 531–538.

[11]Tien, C. L., and Rohani, A. R., "Theory of Two-Component Heat Pipes," *Journal of Heat Transfer*, Vol. 94, Ser. C., No. 4, 1972, pp. 479–484.

[12]Webb, D. R., and Pangoulias, D., "An Improved Approach to Condenser Design Using Film Models," *International Journal of Heat and Mass Transfer*, Vol. 30, No. 2, 1987, pp. 373–378.

[13]Morrison, G., and McLinden, M. O., *Application of a Hard Sphere Equation of State of Refrigerants and Refrigerant Mixtures*, National Bureau of Standards, Gaithersburg, MD, NBS TN-1226, 1986.

[14]Prausnitz, J. M., Lichtenthaler, R. N., and Gomes de Azevedo, E., *Molecular Thermodynamics of Fluid-Phase Equilibria,* Prentice-Hall, Englewood Cliffs, NJ, 1986.

[15]Patankar, S., *Numerical Heat Transfer and Fluid Flow*, Hemisphere, New York, 1980.